Contents lists available at ScienceDirect

Acta Materialia

Full length article

Tellurium self-diffusion in crystalline Ge$_2$Sb$_2$Te$_5$ phase change material

Qingmei Gong [a],[*] , Haihong Jiang [a] , Martin Peterlechner [a],[b] , Sergiy V. Divinski [a] ,
Gerhard Wilde [a]

[a] *University of Münster, Institute of Materials Physics 48149 Münster, Germany*
[b] *Karlsruhe Institute for Technology, Laboratory for Electron Microscopy, Engesserstr. 7 76131 Karlsruhe, Germany*

ARTICLE INFO

ABSTRACT

Ge$_2$Sb$_2$Te$_5$ is the most commonly used material for phase change random access memory. In this work, a chemically homogeneous 200 nm thick layer of amorphous Ge$_2$Sb$_2$Te$_5$ was grown on a single crystal Si wafer using DC magnetron sputtering and applying a stoichiometric target at room temperature. A metastable NaCl-type structure having a face-centered-cubic lattice was obtained by subsequent annealing at 473 K for 30 min. The crystal structure and microstructure were analyzed by X-ray diffraction and transmission electron microscopy. Te self-diffusion was measured by secondary ion mass spectroscopy applying a highly enriched natural ^{122}Te isotope. The Te self-diffusion coefficients follow an Arrhenius law in the temperature range between room temperature and 353 K with an activation enthalpy of (125.0 ± 5) kJ/mol. The diffusion data are discussed in terms of either grain boundary diffusion contributions or, alternatively, in relation to volume diffusion enhanced by structural vacancies. In comparison to the amorphous counterpart, the Te self-diffusion rates in crystalline Ge$_2$Sb$_2$Te$_5$ are only marginally lower and exceed the volume diffusivities of Te in crystalline Te by more than four orders of magnitude, indicating that the structural vacancies seem to determine the measured diffusion rates.

1. Introduction

Phase change memory (PCM) devices represent a rather recent memory technology and are well known for their application in non-volatile and optical rewritable data storage media. Up to now, Ge$_2$Sb$_2$Te$_5$ (GST) still is the most commonly used material in PCMs due to its superior performance, i.e. the high contrast of physical properties between amorphous and crystalline phases, as well as a long cycle lifetime in data processing. To store data, short and intense electrical- or laser pulses are applied, resulting in melting and subsequently quenching the GST into an amorphous phase to achieve data retention. Reversely, data erasing is achieved by the transition from an amorphous to a crystalline state using a pulse of lower intensity but relatively longer duration.

Up to now, numerous efforts have been and are still devoted to studying how to improve the performance of PCM cells, such as a stability improvement of the amorphous state, the optimization of the energy consumption for the reset, and the increase in switching rates [1–3]. Composition variation in the active region is one of the main failure mechanisms induced by the fast atomic mobility during

repetitive transformations between the amorphous and the crystalline phases [4,5]. This behavior leads to detrimental retention of crystalline fractions (low resistance), which negatively affects the data storage [6,7].

The most well-known and most studied crystal structure of GST is the metastable NaCl-type-cubic structure formed above 423 K, in which the standard sites of the face-centered-cubic (FCC) lattice are occupied by Te atoms, while the edge centers and the cell centers are randomly occupied by Ge and Sb atoms. About 20 % of the lattice sites, mainly on the Ge/Sb sublattice [8], are not occupied, resulting in a high concentration of structural vacancies, Fig. 1. When in operation as a phase change memory device, the material is subject to repeated transformations between amorphous and crystalline phases, which is accompanied by changes in volume, resistivity, and optical properties. During these cyclic transformations, it is of high importance to retain a homogeneous chemical composition.

A non-uniform redistribution of atoms induced by atomic migration during repetitive melting and amorphization is one of the main factors to cause reliability problems for PCM devices [9–11]. The new alloy usually has different thermal and electrical properties [4,12]. Besides,
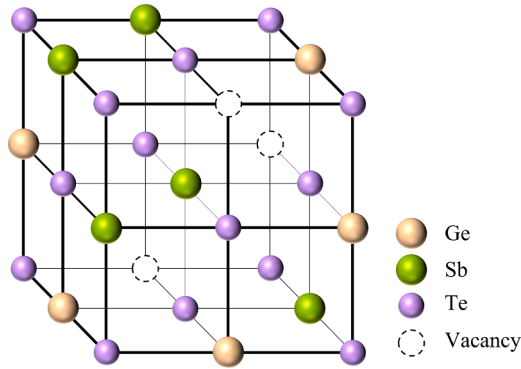

Fig 1. NaCl-type crystal structure of crystalline Ge$_2$Sb$_2$Te$_5$. Te atoms occupy the corner and face center sites of the cubic cell, while Ge, Sb, and vacancies are randomly distributed over the edge centers and the cell center [8].

within the actual memory devices, metal layers are used as electrodes directly contacting the GST layer. The presence of these metal electrodes has important consequences, since in the interfacial region, the interdiffusion of Te in the GST layer and metal atoms in the electrode layer upon heating leads to an irreversible composition modification and the degradation of the microstructure resulting in the early failure of PCMs [13,14]. Under high electrical fields and temperature gradients, the fast atom mobility in the crystalline and molten states causes segregation of Te at the anode, and Sb at the cathode, resulting in a decreased crystallization temperature for GST [9,15]. Therefore, diffusion phenomena not only affect the chemical composition, resulting in a redistribution of atoms, but also further induce microstructure changes that have a direct relation with the variation in electrical and optical properties of the GST [5,16,17].

The investigation of diffusion processes in the crystalline state thus requires further attention. Unfortunately, the literature is scarce regarding diffusion investigations on crystalline GST, especially concerning experimental measurements. The majority of accessible data was obtained by various simulation methods. In nanocrystalline GST, the Te diffusion coefficient was evaluated to be on the order of 10^{-10} m^2/s by ab-initio molecular dynamics simulations at 600 K [2,18]. In a similar temperature range, Novielli et al. [9,19] estimated the diffusivities at about the same order of magnitude and found that the diffusivity in the crystalline phase is much smaller than in the amorphous phase. Experimental investigations of atomic diffusion in the FCC structure are almost absent, probably due to the expected low values of the diffusion coefficients. In a previous work [20], we have measured Te diffusion rates in an amorphous GST phase. By heating above the crystallization temperature, a crystalline GST phase of the same composition is formed, though its diffusion properties were never assessed experimentally.

Therefore, in the present work, the tracer diffusion method in combination with time-of-flight secondary ion mass spectrometry (ToF-SIMS) are utilized to analyze self-diffusion in the crystalline state, even for the small penetration depths of the order of a few tens nanometers only. The diffusion data indicate a strong contribution of structural vacancies to the atomic transport in the crystalline state. A potential contribution of grain boundary (GB) diffusion is carefully analyzed, since the existence of grain boundaries has to be taken into account for the optimization of the resistance in the crystalline state and since the conduction in polycrystalline semiconductors appears to be limited by the grain boundaries [16,21,22].

2. Experimental details

2.1. Synthesis and characterization of GST thin films

Amorphous GST thin films with a thickness of 200 nm were deposited on single-crystalline silicon wafers of (100) orientation with a natural oxide layer via DC magnetron sputter deposition using a stoichiometric target (2 inches in diameter) at room temperature (RT). The thickness of all samples was determined by a profilometer (DektakXT, Bruker). Crystalline GST films were produced via isothermal annealing of as-deposited GST at 473 K for 30 min in a sealed aluminum tube under a highly purified Ar-atmosphere using an oil bath. In addition, films with a 40 nm thickness of GST were directly deposited on a thin amorphous carbon film, which can directly be used for transmission electron microscopy (TEM) characterization. Subsequent to the deposition, the thin films for TEM characterization were also annealed at the abovementioned conditions to obtain a rock-salt structure. Sample transfer was accomplished using a glove-box with a dry Ar-atmosphere and a Gatan vacuum transfer holder.

The structural characterization was carried out using X-ray diffraction (XRD, Siemens D5000) and high-resolution transmission electron microscopy (HR-TEM, Thermo Fisher Scientific, Titan Themis G3 60–300) measurements. All XRD data were collected at RT using Cu-K$_\alpha$ radiation in the 2θ angular range of 20° - 60° with a step size of 0.02°, an integration time of 27 s, and a rotating sample stage. Calibration was performed under the same settings using SiO$_2$ powder.

TEM measurements were conducted at 300 kV applying conventional TEM and scanning-TEM (STEM). Chemical analysis was done by energy-dispersive X-ray spectroscopy (EDS) in STEM mode using all 4 EDS detectors of the Chemi STEM system.

Moreover, non-contact atomic force microscopy (AFM, Park XE-100) was applied to image the surface topography of the thin films on the nanometer scale. The detailed experimental information can be found elsewhere [20].

2.2. Tracer diffusion measurement

A stable ^{122}Te isotope and crystalline GST thin films were utilized for the current diffusion measurements. A thin layer of a highly-enriched (up to 98 %) ^{122}Te isotope (natural abundance of 2.55 %) was deposited on the surface of the crystalline GST film using physical vapor deposition (PVD) at a base pressure below 10^{-5} mbar. An average thickness of 16 nm of the deposited ^{122}Te layer was evaluated by determining the mass gain after the deposition using a microbalance. Subsequently, diffusion annealing treatments were carried out in a sealed aluminum tube under a highly purified Ar-atmosphere using an oil bath. The annealing times and temperatures are listed in Table I.

The ^{122}Te penetration profiles were determined by ToF-SIMS (ION-TOF "ToF-SIMS^5–300") analysis. The reliability of the method for the self- and impurity diffusion measurements was already extensively checked for other materials, see e.g. Refs. [23,24]. This technique is highly sensitive and provides information on the atomic and molecular composition with a nanometer depth resolution and a sensitivity at a ppm level [25]. The lateral resolution is about 100 nm. The final depth of each sputter crater formed during the ToF-SIMS measurements was analyzed with an optical profiler (Sensofar plu Neox) in order to establish the depth scale for evaluating the erosion rate during the analyses. In ToF-SIMS, two different ion beams are used for data acquisition. A sputter beam of Cs$^+$ (500 eV) was employed to erode the specimen, while a second ion beam of Bi$_3^+$ (25 keV) was applied for the chemical characterization of the resulting crater bottom. The data were

Table I
Experimental conditions, temperature T and time t, and the determined ^{122}Te self-diffusion coefficients, D, in crystalline GST thin films.

T (K)	t (10^3 s)	D (m^2/s)
291	2592	$(1.13\pm1.04) \times 10^{-24}$
320	25.2	$(1.60\pm1.56) \times 10^{-22}$
333	1.4	$(1.02\pm0.86) \times 10^{-21}$
343	3.6	$(2.13\pm0.73) \times 10^{-21}$
353	0.42	$(1.19\pm0.60) \times 10^{-20}$

acquired from an area of $100 \times 100\ \mu m^2$, which was chosen from an area larger than $200 \times 200\ \mu m^2$ without any visible defects.

However, the usage of the SIMS technique for self-diffusion studies relies on the availability of natural isotopes with a reasonably small abundance, typically below several percent. In such a fortunate case, i.e. if and only if a corresponding artificially highly-enriched isotope is available, one can use the SIMS technique. This was the case of Te, since the ^{122}Te isotope was at our disposal. Unfortunately, natural Ge and Sb do not have such isotopes. Therefore, in the present work, only the Te diffusion in GST was investigated.

3. Results and discussion

3.1. Microstructure and chemical homogeneity

Isothermal treatments of the as-deposited films at 473 K for 30 min lead to a full crystallization as indicated by the XRD patterns and the HR-TEM image shown in Fig.2. The XRD patterns reveal the presence of a single FCC phase. Moreover, the analysis of the selected area electron diffraction (SAED) pattern (inset in Fig. 2(b)) also reveals that the films have an FCC structure. The lattice constant is evaluated as $a = 5.98 \pm 0.02$ Å, which is in line with reports in the literature [8,26].

The average grain size of polycrystalline GST can be estimated using the Scherrer equation [27,28] in terms of the full width at half maximum (FWHM), β. The FWHM of an XRD peak is related to the domain size (in an undistorted lattice grain size), d, as follows [28],

$$d = \frac{0.89 \times \lambda}{\beta \times \cos\theta} \tag{1}$$

where $\lambda = 0.154056$ nm is the wavelength of the Cu-K$_{\alpha1}$ radiation and θ is the diffraction angle. The (111), (200), (220), and (222) FCC peaks obtained from the XRD patterns in Fig. 2(a) were analyzed and the average domain size of the annealed GST film was found to be (23 ± 8.0) nm.

In order to quantify the grain size distribution in the present crystalline sample, high-angle annular dark-field (HAADF) images were collected by STEM, see Fig. 3(a). A dark-field image highlights the differences in grain orientations within the TEM foil. Thus, comparing to bright-field imaging conditions, GBs appear brightly against a dark background, making them more distinct and convenient to observe and analyse. The longest distance, d_1, and the shortest distance, d_2, within the selected grain were measured using Gatan's "Digital Micrograph" software. Then the average value, $d = (d_1 + d_2)/2$, was considered as the selected grain size. Finally, the average grain size for the polycrystalline GST was evaluated from >100 individual grains. The grain size distribution is presented in Fig. 3(b). The same average grain size, (23 ± 8.5) nm, was obtained from the HAADF-STEM measurements as from the

XRD results. As well known from the literature, the grain size of the FCC structure can range from several nanometers to tens of nanometers [29–32], since the crystallization and grain growth rates sensitively depend on the thermal history of a sample, especially on the temperature ramp-rate [33]. Compared to the grain size distribution of GST annealed at the same temperature, our results are in good agreement with the results reported in the literature [30,31].

As also reported in the literature, atom transport might occur during long-term cycling, thus inducing variations in chemical composition and surface topography, which affects the stability of the PCM devices [34]. In order to analyze the influence of thermal treatments on the element distribution, STEM-EDS analyses were carried out.

The resulting elemental distributions of Ge, Sb, Te, as well as of O in the GST thin films are displayed in Fig. 4. The atomic fractions were averaged over the presented mapping area. Compared with the as-deposited amorphous GST, an increased heterogeneity of the elemental distributions and a relatively higher oxygen content were observed after crystallization. This fact suggests that the chemical composition at the film surface might be modified by the formation of oxides such as GeO_2, Sb_2O_3, and TeO_2 during thermal treatments.

The ToF-SIMS profiles of as-deposited amorphous and crystalline GST films, Fig. 5, substantiate an increased oxygen concentration only near the outer surface, within a layer of < 10 nm in thickness. At larger depths, which are relevant for the present diffusion studies, the corresponding intensity decreases below the detection limit of the ToF-SIMS, Fig.5. The oxides are unavoidably formed on the surface of the GST films, located at the top region in the Te-rich GST layer in the Te/GST diffusion samples. Therefore, the formation of oxides does not have a significant influence on the subsequent diffusion measurements, since our focus is on the diffusion of the ^{122}Te isotope into the crystalline GST beneath the Te-rich GST layer, see a detailed explanation in the diffusion measurement part below. Thus, the small variations of the elemental distribution within the thin subsurface layer after crystallization can safely be neglected in the analysis of the present diffusion measurements.

If only Ge, Sb, and Te are taken into consideration, the chemical composition was evaluated as Ge: Sb: Te = 21.9: 22.4: 55.6 (in at. %), which is close to the nominal composition of $Ge_2Sb_2Te_5$. Thus, the chemical composition is stable in the GST volume and it is not affected by the crystallization of the amorphous phase.

A rather smooth surface morphology was determined by AFM, even though the surface roughness slightly increased after crystallization, from initially 1.0 nm to 1.8 nm after the isothermal treatment at 473 K for 30 min. The relatively small changes of the surface roughness after crystallization might be related to nano-scaled grain size and enhanced surface diffusion. Compared to the intended diffusion lengths, $\sqrt{4Dt} \approx 10$ nm, the surface roughness influences hardly the present measurements of the ^{122}Te diffusion profiles.
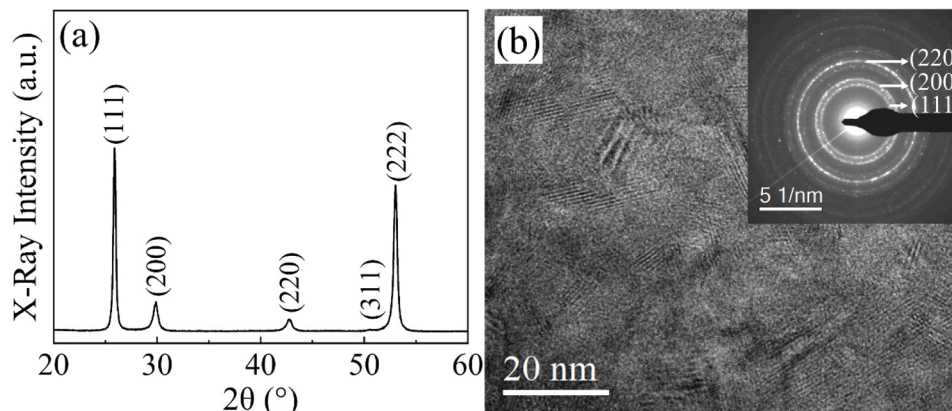

Fig 2. (a) XRD pattern, and (b) HR-TEM image with the SAED pattern (inset) of the thin GST film after annealing at 473 K for 30 min.
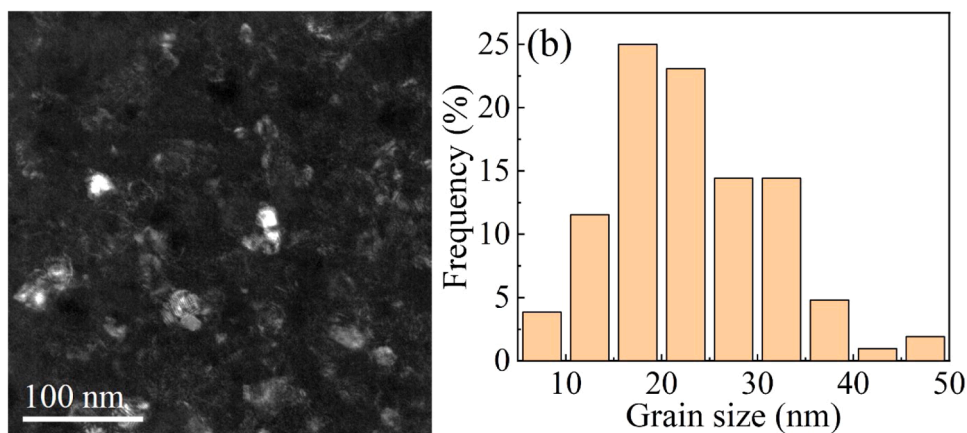
Fig 3. (a)Dark-field image of a GST thin film annealed at 473 K for 30 min and (b) the deduced grain size distribution.
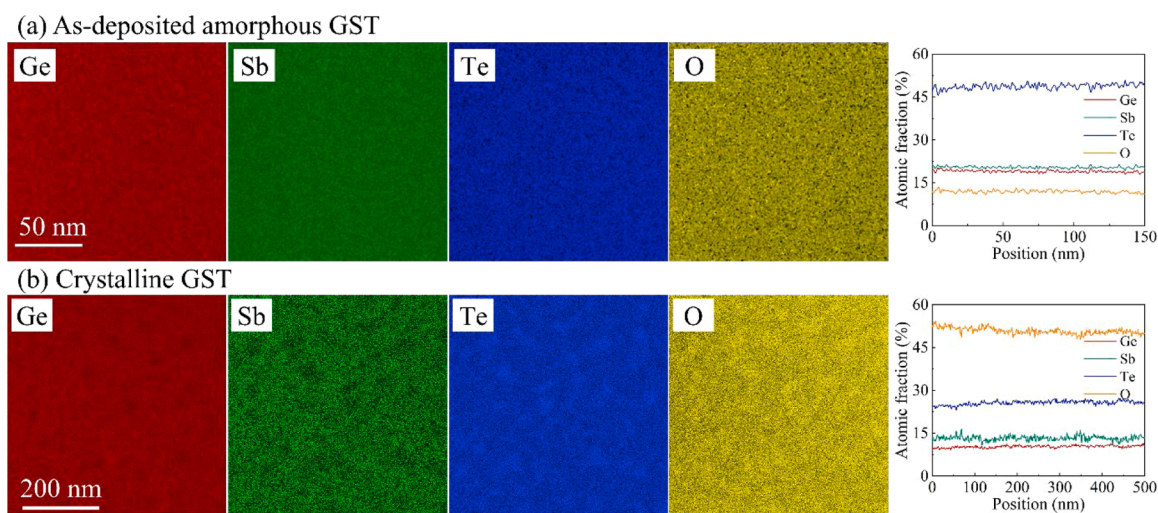

Fig 4. The elemental distribution of (a) vapor-deposited amorphous GST and (b) crystalline GST, and the corresponding line scans of Ge, Sb, Te, and O averaged over the presented mapping area analyzed from STEM-EDS.
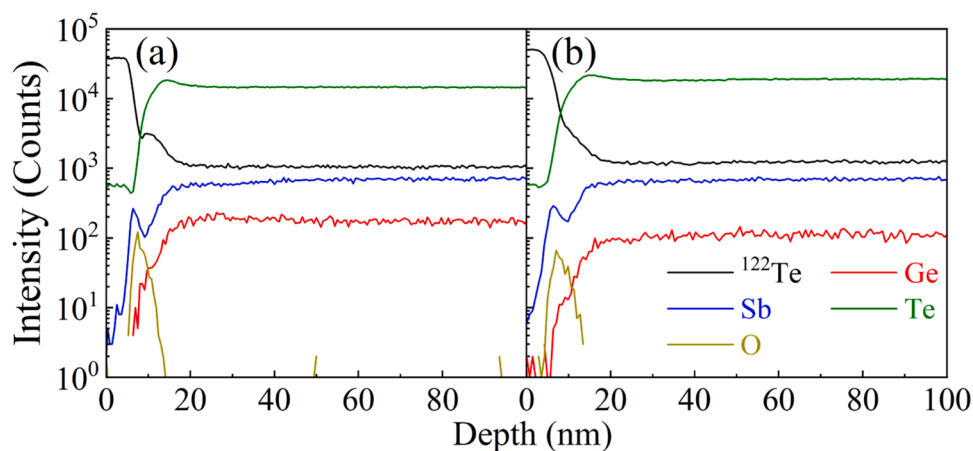

Fig 5. ToF-SIMS depth profiling of Ge, Sb, Te, and O in (a) amorphous GST and (b) FCC GST after ^{122}Te deposition but without any diffusion thermal treatments.

3.2. Tracer diffusion measurements

The ^{122}Te concentration-depth profiles in FCC GST for all diffusion samples obtained by ToF-SIMS are shown in Fig. 6(a). In each case, to rule out a variation of the sputtering rate, the ^{122}Te intensity is normalized on the corresponding ^{128}Te intensity, which is the most abundant isotope in GST and is abbreviated as Te in the present work. The normalized intensity, ^{122}Te/Te, vs. the diffusion depth, x, can be fitted properly by the following equation,

$$C(x,t) = \underbrace{C_1 * \mathrm{erfc}\left(\frac{x-x_1}{2\omega_1}\right)}_{\text{remnant } ^{122}\text{Te layer}} + \underbrace{C_2 * \mathrm{erfc}\left(\frac{x-x_2}{2\omega_2}\right)}_{\text{Te–rich GST layer}} + \underbrace{C_0 * \exp\left(-\frac{(x-x_0)^2}{4b^2}\right)}_{\text{tracer diffusion}} + \underbrace{C_b}_{\text{background}} \tag{2}$$

Here $C(x, t)$ is the concentration of ^{122}Te at the depth x from the surface after the annealing time t; x_i, C_i ($i = 0, 1, 2$), b, ω_1, ω_2 are fitting parameters; C_b is the background value corresponding to the natural abundance of the ^{122}Te isotope in natural Te illustrated by the orange dashed line in Fig. 6(b). erfc(z) is the complementary error function. In the present work, we used the same fitting scheme as in our previous work on amorphous GST [20]. The meaning of all terms in Eq. (2) is directly indicated and the third term is of prime importance (see below for further details).

For a reliable comparison of the diffusion-induced broadening, the origins of the x-axes were set to the positions of the strongest decreases of the tracer concentrations, corresponding to transitions from the erfc-branch to the Gaussian branch of the diffusion profiles. To this end, we systematically selected the origins of the x-axes at ($x_1 - 5$) nm, where x_1 is the fitting parameter from Eq. (2), see Fig. 6.

The fitting results for the as-deposited sample and for a sample obtained after annealing at 320 K for 420 min are shown here as examples to indicate the fitting performance, see Fig. 6(b). The profile shape is similar to those observed in our previous work [20]. It should be noted that the as-deposited sample corresponds to the sample, ^{122}Te/GST, without any diffusion heat treatment.

Thus, just a brief explanation might suffice: the first contribution in Eq. (2) is due to a remnant almost pure ^{122}Te layer (C_1, x_1, ω_1). The second contribution stems from a Te-rich GST layer (C_2, x_2, ω_2) due to the mixing of ^{122}Te with GST produced by PVD deposition of the ^{122}Te isotope. The combined contribution of the first two terms is demonstrated by the green dashed line in Fig. 6(b). The subsequent penetration depth region corresponds to diffusion of the ^{122}Te isotope to the GST matrix and it is fitted by a Gaussian function in Eq. (2), indicated as a blue-dashed line in Fig. 6(b). This contribution represents the true tracer diffusion of ^{122}Te in GST due to diffusion thermal treatments and represents the main focus of the present work. In Fig. 6(c), a linear relationship between the tracer intensity and the square of the penetration depth is shown.

In the as-deposited state, the third term in Eq. (2) corresponds to penetration of the ^{122}Te atoms into crystalline GST during the PVD-deposition. During the ^{122}Te deposition the sample temperature is uncontrolled and moderately increases. The corresponding diffusion process is complex and an analysis of the initial distribution of the ^{122}Te
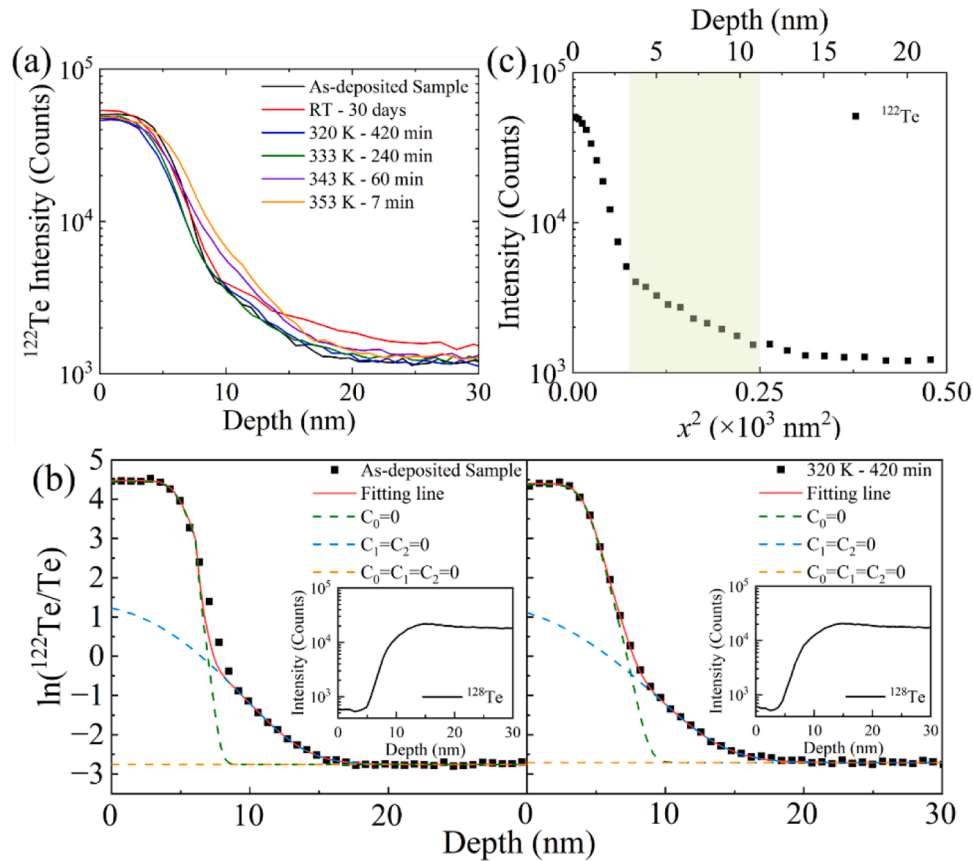
Fig 6. Penetration profiles of ^{122}Te obtained by ToF-SIMS (a) for all diffusion samples under different heat treatment conditions; (b) exemplified individual profiles and decomposed fitting profiles for the as-deposited sample (left) and after diffusion annealing at 320 K for 420 min (right). In (b), the inset images are the corresponding ^{128}Te profiles for each sample; (c) the as-deposited profile is re-plotted in the coordinates of the tracer intensity vs. the penetration depth squared. The remaining profiles for the other samples and the corresponding fitting parameters are shown in the Supplementary Material. Note that for a better comparison, the origin of the depth coordinate is defined as ($x_1 - 5$) nm, see text.

atoms within the GST layer is out of the scope of the present paper. Though, the diffusion-annealing-induced broadening of that term is a reliable parameter for the present analysis.

The tracer diffusion coefficients, D, were determined as $D = \left(b^2 - b_0^2 \right)/t$, here b_0 and b are the corresponding fit parameters in Eq. (2) for the as-deposited sample and for samples after diffusion heat treatments (at the given constant temperatures, T, for the given times, t), respectively. Note that, here, the as-deposited sample was analyzed to account for the influence of the deposition process. The determined diffusion coefficients are listed in Table I.

In Fig. 7, the tracer diffusion coefficients are plotted as a function of the inverse temperature and they are found to follow an Arrhenius-type temperature dependence,

$$D = D_0 \exp\left(-\frac{Q}{RT}\right) \qquad (3)$$

where RT has its usual meaning, Q is the activation energy, D_0 is the pre-exponential factor, which is found to be (0.034 ± 0.062) m^2/s. In the temperature range between 290 K to 355 K, the activation energy, Q, of Te self-diffusion in crystalline GST is evaluated as (125.0 ± 5) kJ/mol.

3.3. Mechanism of Te diffusion in crystalline GST

To the best of our knowledge, no data were reported on diffusion in crystalline GST, although Portavoce with co-authors have estimated a "bulk diffusivity", D_v, in the crystalline GST phase as [36],

$$D_v = \left(C_{Ge}D_0^{Ge} + C_{Sb}D_0^{Sb} + C_{Te}D_0^{Te} \right) \times \exp\left(-\frac{147 \text{ kJ/mol}}{RT}\right) \qquad (4)$$

where C_{Ge}, C_{Sb}, and C_{Te} correspond to the GST composition (in at.%) and the pre-factors (D_0^{Ge}, D_0^{Sb}, and D_0^{Te}) were taken as those for the pure elements. Since self-diffusion in pure Te is the fastest process [36], the corresponding activation energy was used as governing the introduced "bulk diffusivity in GST", Eq. (4). Furthermore, a direct exchange mechanism was considered in corresponding kinetic Monte-Carlo simulations of crystallization and amorphization by Portavoce et al. [36].

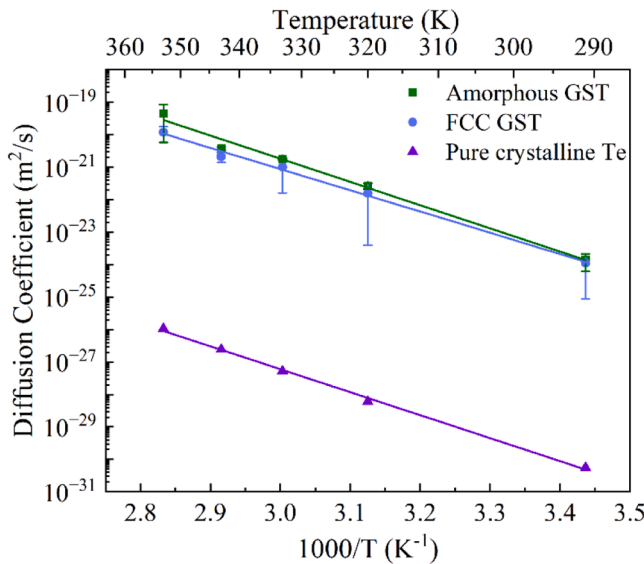In Fig. 7, the measured Te self-diffusion coefficients in pure Te [35]

are compared with the present data on Te diffusion in the crystalline GST phase. Within the temperature interval of the present experiments, the "bulk diffusivity" in GST, estimated by Portavoce et al. via Eq. (4), is slightly lower by a factor of about 0.55 (that essentially corresponds to C_{Te}) than the Te self-diffusion rate in pure Te.

The diffusion coefficients measured in the present experiments exceed those measured by Werner et al. [35] (and used by Portavoce et al. [36]) by more than four orders of magnitude. Note that the melting point of the GST phase, about 900 K [37,38], significantly exceeds that of pure Te, 723 K, and a reverse relation between the diffusion rates might be anticipated. Such a strong enhancement of the Te diffusivity in the GST crystalline phase demands a careful analysis of the possible diffusion mechanism.

Generally, diffusion in the present crystalline GST phase might be enhanced by two reasons:
- a large density of grain boundaries in the crystalline films with an average grain size of about 23 nm;
- the presence of a high concentration of structural vacancies, about 20 %, Fig. 1.

Next, these two possible mechanisms are analyzed in more detail.

3.3.1. Grain boundary diffusion

One may hypothesize [36] that Te in the crystalline bulk of GST diffuses with rates that are about equal to those measured by Werner et al. for self-diffusion in pure Te [35]. It should however be noted that the grain size is rather small, resulting in a high GB fraction, which might enhance the Te diffusion rates, see a schematic in Fig. 8. Note that Huang et al. [5] reported that Te diffusion in crystalline GST might be dominated by grain boundary diffusion, since an enhancement of the atomic migration rates concomitant to an increase of the grain boundary fraction was observed.

The analysis of GB diffusion in a polycrystalline material depends strongly on the corresponding kinetic regime as introduced by Harrison [39]. Under the C-type kinetics, which is relevant for the present case, the logarithm of the tracer concentration has to decay linearly with the penetration depth squared [40] that is supported by the plot in Fig. 6(c). The C-type kinetics conditions are generally fulfilled at lower temperatures, especially at temperatures less than 0.4 T_m (T_m is the melting temperature), and for relatively short diffusion times [40,41].

Formally, the GB diffusion regime can be identified by the value of Le Claire's parameter α [39],

$$\alpha = \frac{s\delta}{2\sqrt{D_v t}} \qquad (5)$$

where s is the segregation factor and δ is the GB width. The value of the segregation factor s might be estimated at about unity for the present case of tracer self-diffusion in the GST materials, since we have not observed a significant enrichment/depletion of Te at grain boundaries.

The value of the GB width δ is usually equal to 0.5 nm for FCC metals and alloys [42,43]. For GST, the value of 0.5 nm was estimated in

Fig 7. Temperature dependence of Te self-diffusion in crystalline GST determined in this work (blue circles and line) in comparison to Te self-diffusion coefficients in pure crystalline Te [35] (purple triangles and line) and the Te self-diffusion coefficients in amorphous GST measured in our previous work [20] (green squares and line).
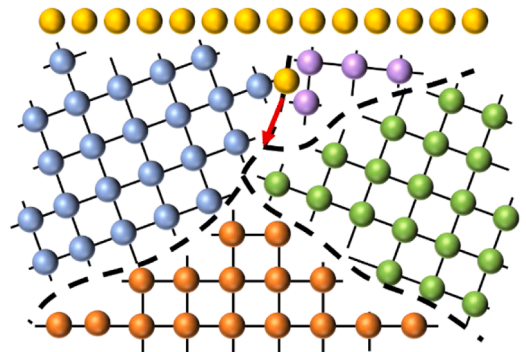

Fig 8. Grain boundary diffusion schema.

simulations of Cueto et al. [44], while Woods et al. [45] estimated the GB width as 2 nm based on simulations of nucleation, growth, and amorphization using a finite element phase-change model.

However, the exact value of δ is not important for the present order-of-magnitude estimates. The C-type kinetics holds when $\alpha \geq 1$, i.e. when the effective GB width, $s \cdot \delta$ exceeds the diffusion penetration depth inside the crystalline bulk. In our work, the penetration profiles of ^{122}Te were measured from RT up to 353 K. In the present conditions, the bulk diffusion depth, $\sqrt{D_v t}$, is estimated to be $< 10^{-3}$ nm, if the estimates of D_v are done using Eq. (4). Therefore, the corresponding value $\alpha \gg 1$ and the C-type kinetics conditions are satisfied.

Thus, we may tentatively assume that the measured Te diffusivities in crystalline GST, Fig.7, correspond to enhanced GB diffusion, while the data of Portavoce et al. [36], Eq. (4), represent volume diffusivity in GST. Having determined the self-diffusion data on GB and bulk diffusion, one may estimate the GB energy, γ_{gb}, using the semiempirical approach by Borisov et al. [46],

$$\gamma_{gb} = \frac{RT}{2a_0^2 N_A} \ln\left(\frac{D_{gb}}{D_v}\right) \tag{6}$$

Here a_0 is the lattice parameter, which is determined as 5.98 Å by XRD measurements, and N_A is Avogadro's number. As a result, the temperature dependence of the GB energy is estimated as,

$$\gamma_{gb} = (0.021 \pm 0.018) + (2.23 \pm 0.55)T \times 10^{-4} \, \text{J}\big/\text{m}^2 \tag{7}$$

At RT, γ_{gb} is then equal to 0.087 J/m^2, while it amounts to 0.216 J/m^2 at the melting temperature of 873 K (T_m is estimated using Ref. [47]).

This estimate cannot be cross-checked due to a lack of available literature data. For the $\Sigma 5$ GB in Ge, a value of 0.482 J/m^2 was obtained by ab-initio calculations [48], while $0.032 \sim 2.53$ J/m^2 was reported as the GB energy for Si [49].

If this interpretation of the measured data is correct, Fig. 7 would suggest that the Te diffusivities in amorphous GST and along the grain boundaries of the crystalline GST phase are nearly the same. This would be in line with original ideas of "amorphous cement" between grains as invented by Brillouin [50] and Quincke [51], although these ideas are not supported by the presently available data [52], see also a recent review [53].

Furthermore, Würschum et al. [54] directly compared the tracer diffusivities along crystalline boundaries and in the residual amorphous phase using Fe as a probe. The results unambiguously suggest that Fe diffuses slower in the amorphous phase as along the inter-crystalline boundaries by two to three orders of magnitude [54].

Thus, we conclude that most probably these are not the grain boundaries, which dominate the diffusion transport in crystalline GST films in the present experiments. Note that the GB diffusion is not inevitably enhanced with respect to the crystalline bulk, as it was e.g. reported for GB diffusion of Au in polycrystalline Si [55,56].

3.3.2. Contribution of structural vacancies

Alternatively to GB diffusion, the relatively fast Te diffusion in crystalline GST, with rates similar to those in the amorphous counterpart, might be induced by a high concentration of structural vacancies, Fig. 1. It is known that in cubic GST, about 20 % vacancies intrinsically exist on the Ge/Sb sublattice [8,57]. Such a larger fraction of vacancies facilitates typically the atomic transport. Still, this statement has to be taken with a care, since, e.g., structural Ni vacancies do not enhance the Ni diffusion rates in B2-ordered NiAl [24], simultaneously increasing the diffusivities of Al [58].

Generally, the activation energy of vacancy self-diffusion consists of two terms, the formation and migration energies of vacancies (typically, the contributions from the temperature dependent correlation factors are small with some important exceptions [40]). From the analysis of a molecular dynamics simulation [59], the formation energy of thermal

vacancies on the Te sublattice was found as about 96 kJ/mol, while those on the Sb and Ge sublattice are about 34 and 60 kJ/mol, respectively. The activation energy of vacancy-mediated element jumps is < 96 kJ/mol in crystalline GST [60]. These estimates are in an acceptable agreement with the present experimental data, especially accounting for the existence of structural vacancies which reduce the energy penalties for atomic motion and a potential contribution of strong correlation effects in an ordered compound. A further analysis would require ab-initio informed calculations of intrinsic defects and a detailed evaluation of the atomistic mechanisms enabling long-range diffusion of Te atoms. At this moment, we may speculate only about potential diffusion mechanism(s) in this compound. Anions might diffuse as self-interstitials or using anion vacancies jumping via, e.g., the body-interstitial sites [61,62]. Another possible anion diffusion mechanism is through Schottky defects or vacancy pairs (anion-cation di-vacancy), which can predominate when the concentration of Schottky defects is significant [63,64]. Furthermore, formation of intrinsic defects on the anion sublattice near the structure cation vacancies and the contribution of interstitial Te atoms in such extrinsic conditions have to be properly analysed [65]. We left such analysis for a future work.

4. Conclusions

In the present work, Te self-diffusion in polycrystalline GST was measured in the temperature interval between RT to 353 K using a highly enriched ^{122}Te isotope as a tracer and applying the ToF-SIMS technique. The microstructure of the polycrystalline material was determined by XRD and TEM characterization, and an average grain size of 23 nm was evaluated. Self-diffusion coefficients between $10^{-24} \sim 10^{-20}$ m^2/s were found to follow an Arrhenius-type dependence with an activation energy of (125.0 ± 5) kJ/mol.

The determined data have been analyzed in detail based on two alternative models based on either the presence of a dominant contribution from enhanced GB diffusion or a strong contribution of structural vacancies. The current work in conjunction with existing analyses based on simulation results strongly suggests that the diffusion contribution due to the presence of a large fraction of structural vacancies dominates the enhancement of the self-diffusion rate of Te in crystalline GST.

The reported observations here have important consequences for the reliability optimization of PCM devices. The study on diffusion mechanisms may provide beneficial information to understand the degradation of active PCM cells.

CRediT authorship contribution statement

Qingmei Gong: Conceptualization, Data curation, Formal analysis, Investigation, Methodology, Validation, Visualization, Writing – original draft, Writing – review & editing. **Haihong Jiang:** Conceptualization, Data curation, Formal analysis, Investigation, Methodology, Validation, Visualization, Writing – original draft, Writing – review & editing. **Martin Peterlechner:** Data curation, Formal analysis, Methodology, Writing – original draft, Writing – review & editing. **Sergiy V. Divinski:** Conceptualization, Formal analysis, Investigation, Methodology, Supervision, Writing – original draft, Writing – review & editing. **Gerhard Wilde:** Conceptualization, Funding acquisition, Investigation, Supervision, Visualization, Writing – original draft, Writing – review & editing.

Declaration of competing interest

The authors declare that they have no known competing financial interests or personal relationships that could have appeared to influence the work reported in this paper.

Acknowledgments

Supplementary materials

Supplementary material associated with this article can be found, in the online version, at doi:10.1016/j.actamat.2025.120929.

References

[1] Y. Xue, S. Song, X. Chen, S. Yan, S. Lv, T. Xin, Z. Song, Enhanced performance of phase change memory by grain size reduction, J. Mater. Chem. C 10 (2022) 3585, https://doi.org/10.1039/D1TC06045G.

[2] J. Shen, T. Li, X. Chen, S. Jia, S. Lv, L. Li, Z. Song, M. Zhu, Dynamic evolution of thermally induced element distribution in nitrogen modified phase change materials, J. Appl. Phys. 128 (2020) 075701, https://doi.org/10.1063/5.0006519.

[3] S. Kumar, V. Sharma, Improvement in thermal stability and crystallization mechanism of Sm doped Ge2Sb2Te5 thin films for phase change memory applications, J. Alloy Compd. 893 (2022) 162316, https://doi.org/10.1016/j.jallcom.2021.162316.

[4] M.A. Luong, S. Ran, M. Bernard, A. Claverie, An experimental study of ge diffusion through Ge2Sb2Te5, Mat. Sci. Semicon. Proc. 152 (2022) 107101, https://doi.org/10.1016/j.mssp.2022.107101.

[5] Y.-H. Huang, C.-H. Hang, Y.-J. Huang, T.-E. Hsieh, Electromigration behaviors of Ge2Sb2Te5 chalcogenide thin films under dc bias, J. Alloy. Compd. 580 (2013) 449, https://doi.org/10.1016/j.jallcom.2013.06.129.

[6] S.-H. Hong, H. Lee, Failure analysis of Ge2Sb2Te5 based phase change memory, Jpn. J. Appl. Phys. 47 (2008) 3372, https://doi.org/10.1143/JJAP.47.3372.

[7] S. Lee, J.-h. Jeong, T.S. Lee, W.M. Kim, B.-k. Cheong, A study on the failure mechanism of a phase-change memory in write/erase cycling, IEEE Electr. Dev. L 30 (2009) 448, https://doi.org/10.1109/LED.2009.2015222.

[8] N. Yamada, T. Matsunaga, Structure of laser-crystallized Ge2Sb2+xTe5 sputtered thin films for use in optical memory, J. Appl. Phys. 88 (2000) 7020, https://doi.org/10.1063/1.1314323.

[9] T.-Y. Yang, I.-M. Park, B.-J. Kim, Y.-C. Joo, Atomic migration in molten and crystalline Ge2Sb2Te5 under high electric field, Appl. Phys. Lett. 95 (2009) 032104, https://doi.org/10.1063/1.3184584.

[10] Y.-J. Park, T.-Y. Yang, J.-Y. Cho, S.-Y. Lee, Y.-C. Joo, Electrical current-induced gradual failure of crystalline Ge2Sb2Te5 for phase-change memory, Appl. Phys. Lett. 103 (2013) 073503, https://doi.org/10.1063/1.4818684.

[11] A. Debunne, K. Virwani, A. Padilla, G.W. Burr, A.J. Kellock, V.R. Deline, R. M. Shelby, B. Jackson, Evidence of crystallization–induced segregation in the phase change material Te-rich GST, J. Electrochem. Soc. 158 (2011) https://doi.org/10.1149/1.3614508. H965.

[12] G. D'Arrigo, A. Mio, M. Boniardi, A. Redaelli, E. Varesi, S. Privitera, G. Pellegrino, C. Spinella, E. Rimini, Crystallization properties of Sb-rich GeSbTe alloys by in-situ morphological and electrical analysis, Mat. Sci. Semicon. Proc. 65 (2017) 100, https://doi.org/10.1016/j.mssp.2016.07.014.

[13] L. Lu, W. Dong, J.K. Behera, L. Chew, R.E. Simpson, Inter-diffusion of plasmonic metals and phase change materials, J. Mater. Sci. 54 (2019) 2814, https://doi.org/10.1007/s10853-018-3066-x.

[14] S. Alberici, R. Zonca, B. Pashmakov, Ti diffusion in chalcogenides: a ToF-SIMS depth profile characterization approach, Appl. Surf. Sci. 231 (2004) 821, https://doi.org/10.1016/j.apsusc.2004.03.129.

[15] Y.J. Park, J.Y. Lee, M.S. Youm, Y.T. Kim, Effects of annealing conditions on the crystallization and grain growth of metastable Ge2Sb2Te5, Jpn. J. Appl. Phys. 44 (2005) 326, https://doi.org/10.1143/JJAP.44.326.

[16] N. Ciocchini, E. Palumbo, M. Borghi, P. Zuliani, R. Annunziata, D. Ielmini, Modeling resistance instabilities of set and reset states in phase change memory with Ge-rich GeSbTe, IEEE T Electron. Dev. 61 (2014) 2136, https://doi.org/10.1109/TED.2014.2313889.

[17] N. Ciocchini, E. Palumbo, M. Borghi, P. Zuliani, R. Annunziata, D. Ielmini, Unified reliability modeling of Ge-rich phase change memory for embedded applications, in: 2013 IEEE International Electron Devices Meeting, IEEE, 2013, https://doi.org/10.1109/IEDM.2013.6724681, 22–1.

[18] T. Li, J. Shen, L. Wu, Z. Song, S. Lv, D. Cai, S. Zhang, T. Guo, S. Song, M. Zhu, Atomic-scale observation of carbon distribution in high-performance carbon-doped Ge2Sb2Te5 and its influence on crystallization behavior, J. Phys. Chem. C 123 (2019) 13377, https://doi.org/10.1021/acs.jpcc.9b02098.

[19] G. Novielli, A. Ghetti, E. Varesi, A. Mauri, R. Sacco, Atomic migration in phase change materials, in: 2013 IEEE International Electron Devices Meeting, IEEE, 2013, pp. 22–23, https://doi.org/10.1109/IEDM.2013.6724683.

[20] Q. Gong, H. Jiang, J. Perrin-Toinin, M. Peterlechner, M. Putero, A. Portavoce, S. Divinski, G. Wilde, Tellurium self-diffusion in amorphous Ge2Sb2Te5 phase change materials, Acta Mater. (2023) 119146, https://doi.org/10.1016/j.actamat.2023.119146.

[21] M.M. Mandurah, K.C. Saraswat, T.I. Kamins, A model for conduction in polycrystalline silicon-part i: theory, IEEE T Electron. Dev. 28 (1981) 1163, https://doi.org/10.1109/T-ED.1981.20504.

[22] C. Angelis, C. Dimitriadis, I. Samaras, J. Brini, G. Kamarinos, V. Gueorguiev, T. E. Ivanov, Study of leakage current in n-channel and p-channel polycrystalline silicon thin-film transistors by conduction and low frequency noise measurements, J. Appl. Phys. 82 (1997) 4095, https://doi.org/10.1063/1.365720.

[23] K. Maier, H. Mehrer, E. Lessmann, W. Schüle, Self-diffusion in nickel at low temperatures, Phys. Stat. Solidi B 78 (1976) 689, https://doi.org/10.1002/pssb.2220780230.

[24] S. Frank, S. Divinski, U. Södervall, C. Herzig, Ni tracer diffusion in the B2-compound NiAl: influence of temperature and composition, Acta Mater. 49 (2001) 1399, https://doi.org/10.1016/S1359-6454(01)00037-4.

[25] P. Bertrand, W. Lu-Tao, Time-of-flight Secondary Ion Mass Spectrometry (ToF-SIMS), in Microbeam and Nanobeam Analysis, Springer, Vienna, 1996, pp. 167–182, https://doi.org/10.1007/978-3-7091-6555-3_8.

[26] I. Friedrich, V. Weidenhof, W. Njoroge, P. Franz, M. Wuttig, Structural transformations of Ge2Sb2Te5 films studied by electrical resistance measurements, J. Appl. Phys. 87 (2000) 4130, https://doi.org/10.1063/1.373041.

[27] A. Patterson, The scherrer formula for x-ray particle size determination, Phys. Rev. 56 (1939) 978, https://doi.org/10.1103/PhysRev.56.978.

[28] J.I. Langford, A. Wilson, Scherrer after sixty years: a survey and some new results in the determination of crystallite size, J. Appl. Crystallogr. 11 (1978) 102, https://doi.org/10.1107/S0021889878012844.

[29] J. Xu, C. Qi, L. Chen, L. Zheng, Q. Xie, The microstructural changes of Ge2Sb2Te5 thin film during crystallization process, AIP Adv. 8 (2018) 055006, https://doi.org/10.1063/1.5025204.

[30] L. Adnane, F. Dirisaglik, A. Cywar, K. Cil, Y. Zhu, C. Lam, A. Anwar, A. Gokirmak, H. Silva, High temperature electrical resistivity and seebeck coefficient of Ge2Sb2Te5 thin films, J. Appl. Phys. 122 (2017) 125104, https://doi.org/10.1063/1.4996218.

[31] Y.-H. Huang, Y.-J. Huang, T.-E. Hsieh, A study of phase transition behaviors of chalcogenide layers using in situ alternative-current impedance spectroscopy, J. Appl. Phys. 111 (2012) 123706, https://doi.org/10.1063/1.4729528.

[32] H.S.H. Seo, T.-H.J.T.-H. Jeong, J.-W.P.J.-W. Park, C.Y.C. Yeon, S.-J.K.S.-J. Kim, S.-Y.K.S.-Y. Kim, Investigation of crystallization behavior of sputter-deposited nitrogen-doped amorphous Ge2Sb2Te5 thin films, Jpn. J. Appl. Phys. 39 (2000) 745, https://doi.org/10.1143/JJAP.39.745.

[33] G.W. Burr, P. Tchoulfian, T. Topuria, C. Nyffeler, K. Virwani, A. Padilla, R. M. Shelby, M. Eskandari, B. Jackson, B.-S. Lee, Observation and modeling of polycrystalline grain formation in Ge2Sb2Te5, J. Appl. Phys. 111 (2012) 104308, https://doi.org/10.1063/1.4718574.

[34] Y. Wang, X. Chen, Y. Cheng, X. Zhou, S. Lv, Y. Chen, Y. Wang, M. Zhou, H. Chen, Y. Zhang, et al., Reset distribution improvement of phase change memory: the impact of pre-programming, IEEE Electr. Device. L 35 (2014) 536, https://doi.org/10.1109/LED.2014.2308909.

[35] M. Werner, H. Mehrer, H. Siethoff, Self-diffusion and antimony diffusion in tellurium, Solid State Phys. 16 (1983) 6185, https://doi.org/10.1088/0022-3719/16/32/011.

[36] A. Portavoce, G. Roland, J. Remondina, M. Descoins, M. Bertoglio, M. Amalraj, P. Eym'eoud, D. Dutartre, F. Lorut, M. Putero, Kinetic monte carlo simulations of Ge-Sb-Te thin film crystallization, Nanotechnology. 33 (2022) 295601, https://doi.org/10.1088/1361-6528/ac6813.

[37] B. Legendre, C. Hancheng, S. Bordas, M. Clavaguera-Mora, Phase diagram of the ternary system Ge-Sb-Te. I. The subternary GeTe-Sb2Te3-Te, Thermochim. Acta 78 (1984) 141, https://doi.org/10.1016/0040-6031(84)87142-7.

[38] S. Bordas, M. Clavaguer-Mora, B. Legendre, C. Hancheng, Phase diagram of the ternary system Ge-Sb-Te: II. The subternary Ge-GeTe-Sb2Te3-Sb, Thermochim. Acta 107 (1986) 239, https://doi.org/10.1016/0040-6031(86)85051-1.

[39] L. Harrison, Influence of dislocations on diffusion kinetics in solids with particular reference to the alkali halides, Trans. Faraday Soc. 57 (1961) 1191, https://doi.org/10.1039/tf9615701191.

[40] A. Paul, T. Laurila, V. Vuorinen, S.V. Divinski, Thermodynamics, Diffusion and the Kirkendall effect in Solids, Springer, 2014, https://doi.org/10.1007/978-3-319-07461-0.

[41] I. Kaur, Y. Mishin, W. Gust, Fundamentals of Grain and Interphase Boundary Diffusion, John Wiley, 1995.

[42] S.V. Divinski, G. Reglitz, G. Wilde, Grain boundary self-diffusion in polycrystalline nickel of different purity levels, Acta Mater. 58 (2010) 386, https://doi.org/10.1016/j.actamat.2009.09.015.

[43] D. Prokoshkina, V. Esin, G. Wilde, S. Divinski, Grain boundary width, energy and self-diffusion in nickel: effect of material purity, Acta Mater. 61 (2013) 5188, https://doi.org/10.1016/j.actamat.2013.05.010.

[44] O. Cueto, V. Sousa, G. Navarro, and S. Blonkowski, Coupling the phase-field method with an electrothermal solver to simulate phase change mechanisms in pcram cells, in 2015 International Conference on Simulation of Semiconductor Processes and Devices (SISPAD) (IEEE, 2015) pp. 301–304, https://doi.org/10.1109/SISPAD.2015.7292319.

[45] Z. Woods, J. Scoggin, A. Cywar, A. Gokirmak, et al., Modeling of phase-change memory: nucleation, growth, and amorphization dynamics during set and reset: part ii-discrete grains, IEEE T Electron. Dev. 64 (2017) 4472, https://doi.org/10.1109/TED.2017.2745500.

[46] V. Borisov, V. Golikov, G. Scherbedinskiy, Relation between diffusion coefficients and grain boundary energy, Fiz. Met. Metalloved. 17 (1964) 881.

[47] T. Kato, K. Tanaka, Electronic properties of amorphous and crystalline Ge2Sb2Te5 films, Jpn. J. Appl. Phys. 44 (2005) 7340, https://doi.org/10.1143/JJAP.44.7340.

[48] E. Tarnow, P. Bristowe, J. Joannopoulos, M. Payne, Predicting the structure and energy of a grain boundary in germanium, J. Phys. Condens. Matter. 1 (1989) 327, https://doi.org/10.1088/0953-8984/1/2/001.

[49] S. Ratanaphan, Y. Yoon, G.S. Rohrer, The five parameter grain boundary character distribution of polycrystalline silicon, J. Mater. Sci. 49 (2014) 4938, https://doi.org/10.1007/s10853-014-8195-2.

[50] M. Brillouin, Théorie des déformations permanentes des métaux industriels, Ann. Chem. Phys. 13 (1898) 77.

[51] G. Quincke, The formation of ice and the grained structure of glaciers, Proc. Roy. Soc. (Lond.) A 76 (1905) 431, https://doi.org/10.1098/rspa.1905.0048.

[52] H. Gleiter, The structure and properties of high-angle grain boundaries in metals, Phys. Status. Solidi B 45 (1971) 9, https://doi.org/10.1002/pssb.2220450102.

[53] S. Patala, Understanding grain boundaries – The role of crystallography, structural descriptors and machine learning, Comp. Mater. Sci. 162 (2019) 281, https://doi.org/10.1016/j.commatsci.2019.02.047.

[54] R. Würschum, T. Michel, P. Scharwaechter, W. Frank, H.-E. Schaefer, Fe diffusion in nanocrystalline alloys and the influence of amorphous intergranular layers, Nanostruct. Mater. 12 (1999) 555, https://doi.org/10.1016/S0965-9773(99)00182-8.

[55] C. Poisson, A. Rolland, J. Bernardini, N.A. Stolwijk, Diffusion of gold into polycrystalline silicon investigated by means of the radiotracer 195Au, J. Appl. Phys. 80 (1996) 6179, https://doi.org/10.1063/1.363712.

[56] N.A. Stolwijk, C. Poisson, J. Bernardini, Segregation-controlled kinetics of fast impurity diffusion in polycrystalline solids, J. Phys. Condens. Matter. 8 (1996) 5843, https://doi.org/10.1088/0953-8984/8/32/005.

[57] A. Lotnyk, S. Bernütz, X. Sun, U. Ross, M. Ehrhardt, B. Rauschenbach, Real-space imaging of atomic arrangement and vacancy layers ordering in laser crystallised Ge2Sb2Te5 phase change thin films, Acta Mater. 105 (2016) 1–8, https://doi.org/10.1016/j.actamat.2015.12.010.

[58] Y. Minamino, Y. Koizumi, Y. Inui, In diffusion in B2-type ordered NiAl intermetallic compound in diffusion in materials DIMAT2000, Defect and Diffusion Forum, Trans. Tech. Public. Ltd 194 (2001) 517–522, https://doi.org/10.4028/www.scientific.net/DDF.194-199.517.

[59] S. Caravati, M. Bernasconi, T.K ühne, M. Krack, M. Parrinello, First-principles study of crystalline and amorphous Ge2Sb2Te5 and the effects of stoichiometric defects, J. Phys. Condens. Matter. 21 (2009) 255501, https://doi.org/10.1088/0953-8984/21/25/255501.

[60] B. Zhang, W. Zhang, Z. Shen, Y. Chen, J. Li, S. Zhang, Z. Zhang, M. Wuttig, R. Mazzarello, E. Ma, et al., Element-resolved atomic structure imaging of rocksalt Ge2Sb2Te5 phase-change material, Appl. Phys. Lett. 108 (2016) 191902, https://doi.org/10.1063/1.4949011.

[61] M. Kuklja, E. Kotomin, A. Popov, Semi-empirical simulations of F-center diffusion in KCl crystals, J. Phys. Chem. Solids. 58 (1997) 103–106, https://doi.org/10.1016/S0022-3697(96)00096-0.

[62] N. Mishra, G. Makov, Modelling diffusion in large anion binary rock-salt compounds, Mater. Chem. Phys. 305 (2023) 128004, https://doi.org/10.1016/j.matchemphys.2023.128004.

[63] M. Yang, C. Flynn, Intrinsic diffusion properties of an oxide: mgO, Phys. Rev. Lett. 73 (1994) 1809, https://doi.org/10.1103/PhysRevLett.73.1809.

[64] N. Mishra, G. Makov, Point defects in lead sulfide: a frst-principles study, Comp. Mater. Sci. 190 (2021) 110285, https://doi.org/10.1016/j.commatsci.2021.110285.

[65] H. Schmalzried, Chemic. Kin. Solids (1995), https://doi.org/10.1002/9783527615537.